

Metal–Insulator Phenomena in Strongly Correlated Oxides. The Vacancy-Doped Titanate Perovskites, $\text{Nd}_{1-x}\text{TiO}_3$ and $\text{Sm}_{1-x}\text{TiO}_3$

G. Amow, N. P. Raju, and J. E. Greedan¹*Brockhouse Institute for Materials Research, McMaster University, Hamilton, Ontario, L8S 4M1 Canada*

Received June 2, 2000; in revised form August 1, 2000; accepted August 15, 2000

DEDICATED TO PROFESSOR J. M. HONIG

INTRODUCTION

Electrical transport, both resistivity and thermopower, and heat capacity data are reported for two systems of cation vacancy-doped titanate perovskites, $\text{Nd}_{1-x}\text{TiO}_3$ and $\text{Sm}_{1-x}\text{TiO}_3$. In the former case the range of x is from 0.33 to 0.00 and for the latter from 0.17 to 0.00. Thus, the nominal carrier concentration, n , can be varied from 0 ($x = 0.33$) to 1.0 ($x = 0.00$) electrons per Ti atom. For the Nd series two distinct metal–insulator transitions (MIT) are seen, one obtained by electron doping the charge-transfer insulator, CTI ($x = 0.33$), which occurs at $x \sim 0.20$, and the other by hole doping the Mott–Hubbard insulator, MHI ($x = 0.00$), which is found near $x \sim 0.10$. Beginning near the CTI composition, $x = 0.30$, evidence is found for variable range hopping from both resistivity and thermopower data. Mott metallization occurs near $x = 0.20$ and Fermi-liquid (FL) behavior (T^2 dependence of the resistivity) is seen between $x = 0.20$ and 0.10. The coefficient of the T^2 term increases with decreasing x (increasing n) and attains a large value, $3.0 \times 10^{-8} \Omega\text{-cm K}^{-2}$, for $x \sim 0.12$, which is more than 10 times larger than values seen in other titanate systems. Correspondingly large values for the heat capacity γ are observed. The $x = 0.10$ sample shows a remarkable resistivity temperature dependence with a maximum at ~ 175 K and minimum at ~ 50 K followed by an upturn at the lowest temperatures. This is similar to behavior seen for Kondo or valence-fluctuating materials and is qualitatively consistent with existing theory, which predicts a Kondo-like transition state between the FL and MHI regimes. The $x = 0.05$ and ~ 0.00 are hole-doped antiferromagnetic semiconductors but thermopower data for the former shows a change from p- to n-type carriers just near 300 K. $\text{Sm}_{1-x}\text{TiO}_3$ is even more unusual as only the p-type semiconducting and the Kondo-like conducting regimes are seen. Comparisons are drawn with related $\text{Ln}_{1-x}\text{A}_x\text{TiO}_3$ and $\text{Ln}_{1-x}\text{TiO}_3$ series and the role of correlation is emphasized. © 2000

Academic Press

Key Words: titanates; electron correlation; Mott Hubbard insulator; metal–insulator; transition; Fermi-liquid; Kondo.

Materials exhibiting unexpected properties due to the dominant effect of strong electronic correlations have attracted interest for a very long time, beginning, perhaps, with the observation that simple transition metal compounds such as NiO, which should be metallic conductors according to one electron band theory, are in fact antiferromagnetic insulators (1). A conceptual framework for understanding the role of electron correlation was introduced by Mott (2) and Hubbard (3) through the electron correlation parameter, U . In the simplest interpretation, U is the energy cost of placing two electrons at the same orbital site or the cost of transferring an electron between two half-filled orbital sites. In the limit of zero intersite interaction, the “activation energy” for electron transport is exactly U . For non-zero interactions, the two states, before and after the electron transfer, are broadened into quasi-particle bands called the lower (LHB) and upper (UHB) Hubbard bands, respectively, of a width, W . Thus, if $U > W$, the LHB and UHB will not overlap and the material will be insulating, whereas if $W > U$, there will be a finite overlap and a metallic ground state will result. Spin–spin correlations that arise through the Pauli principle serve to render the insulating ground state antiferromagnetic.

More recently, Zaanen, Sawatsky, and Allen (ZSA) have extended these ideas by introducing a charge-transfer energy, Δ , which is the cost of exciting an electron from a filled band associated with the highest occupied ligand states to the lowest unoccupied metal state, usually the UHB (4). In the ZSA scheme there are two types of insulating ground state, the charge-transfer insulator (CTI) for which $U > \Delta > W$ and the original Mott–Hubbard insulator for which $\Delta > U > W$. Usually, for transition metal compounds, the CTI description is appropriate for elements near the end of the series, e.g., Ni, Cu, while the MHI picture seems to hold for elements near the beginning of the series, e.g., Ti, V.

Among the classes of transition metal compounds with strong electronic correlations, oxides have been the most

¹ To whom correspondence should be addressed. Fax: (905) 521-2773. E-mail: greedan@mcmaster.ca.

extensively studied. This is due to the fact that, for the oxide ligand, the ZSA parameters, Δ , U , and W are close in energy and the relative magnitudes can be manipulated through changes in materials chemistry. Initially, binary oxides such as NiO and V_2O_3 received much attention, but more recently, the focus has been on more complex chemical systems and in particular those with perovskite or perovskite-related structures. The most prominent examples are of course the cuprate superconductors such as $La_{2-x}CuO_4$, $YBa_2Cu_3O_7$, and many others. In these materials a CTI phase, La_2CuO_4 or $YBa_2Cu_3O_7$ for example, can be hole-doped to induce a metal-insulator transition and further doping leads to the superconducting state. Other CTI materials such as La_2NiO_4 can also be hole-doped but instead of a superconducting state, there is some evidence that a phase separation occurs, resulting in spatially distinct domains that are alternately metallic or insulating, the so-called stripe domains (5).

Extensive studies of doped MHI perovskites have also been carried out. One set of materials that has drawn much interest is the $LnTiO_3$ series, where Ln is a rare earth and Ti has configuration $3d^1$. The MHI character of these materials has been well established by optical measurements that clearly show that $\Delta > U > W$ (6). The MH gap can be tuned by changing the Ln ion, the gap magnitude decreasing with increasing Ln^{3+} radius (7). This is best understood in terms of the crystal structure of these compounds in which the Ti–O–Ti bond angle, which controls the bandwidth, W , decreases with decreasing Ln^{3+} radius (8). As U will be a constant, roughly, for this series the ratio U/W , which can be called a correlation index, is therefore tunable.

Doping of these materials to induce metal-insulator transitions is done, typically, by substitution of a divalent cation, A , of roughly the same radius as the trivalent Ln ion. In most cases a more or less continuous “solid solution”, $Ln_{1-x}A_xTiO_3$ exists between the end members, $ATiO_3$ with a d^0 configuration at Ti and $LnTiO_3$ with a d^1 configuration. Thus, at the $ATiO_3$ end one has a CTI and at the $LnTiO_3$ end a MHI. Therefore, two metal-insulator transitions, MITs, are expected, one obtained by electron doping of $ATiO_3$ and one by hole-doping of $LnTiO_3$. A generalized phase diagram depicting this situation is shown in Fig. 1. Beginning at the CTI side (carrier/atom, $n = 0$), a MIT should occur at a critical n , $n_c(1)$, for which the carrier density is sufficient to screen the carriers from the effect of U according to the arguments of Mott (9). On the insulating side of $n_c(1)$, an activated conductivity is expected due to electron hopping or small polaron behavior. If the disorder induced by the chemical doping, A^{2+}/Ln^{3+} , is a sufficient perturbation, variable range hopping (VRH) may be found (10). On the metallic side of $n_c(1)$, correlated metallic or Fermi-liquid behavior is expected (11).

The situation near the second MIT boundary, $n_c(2)$ is less clear. Approaching from the metallic side, a diverging effec-

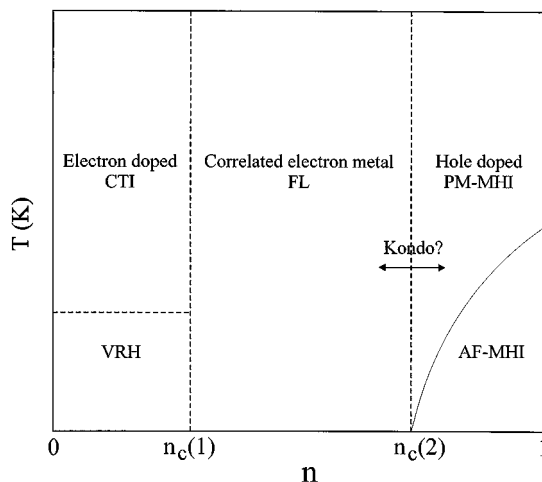


FIG. 1. A possible electronic phase diagram for a CTI-MHI system between $n = 0$ and $n = 1$.

tive mass should be seen with increasing n (11). Beginning at the $n = 1$ MHI end, $LnTiO_3$ hole-doping will result in the destruction of the AF magnetic order at a concentration that may or may not coincide with $n_c(2)$. The situation near $n_c(2)$ is also unclear. Both theories in the somewhat artificial limit of infinite dimensions and Monte Carlo simulations indicate that a Kondo-like state may be an intermediate in the transition between the MHI and FL regimes (12). This is in contrast to the case of hole-doped CTIs with primarily two-dimensional electronic structures, where the stripe phenomenon, referred to earlier, has been postulated to occur.

The main features of Fig. 1, just described, have been found in studies of a number of $Ln_{1-x}A_xTiO_3$ systems where $A = Ca$ or Sr and $Ln = La, Nd, Sm, \text{ or } Y$ (13). As an alternative to doping the Ln site with divalent ions, doping with Ln vacancies has also been explored (14). This mode is possible due to the existence of phases of composition $Ln_{2/3}TiO_3$, for which $n = 0$, which have a perovskite-related structure (14). The crystallography of this structure type has been described for $Ln = La$ and Nd and the structural trends for $Ln_{1-x}TiO_3$ have been established for $Ln = La, Nd, \text{ and } Sm$ over the relevant range, $0.0 < x < 0.33$ (14, 15). To summarize these, the $Ln_{2/3}TiO_3$ phase is described in Pbn and the Ln vacancies are ordered, primarily on one of two sites. $LnTiO_3$ crystallizes in $Pnma$ with one Ln site. A more or less continuous solid solution exists between the two perovskite-related end members. For increasing x (decreasing n) the average Ti–O distance decreases and the average Ti–O–Ti angle increases. Both of these trends imply increasing W for increasing x . On the other hand, as x increases, the concentration of Ln vacancies increases. Thus, the level of disorder also increases, which may mitigate in part the increase in W expected from the distance/angle correlations just described. It is, therefore, not straightforward to predict the effects of increasing x on the correlation

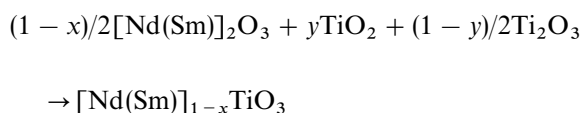
index, U/W , for the same Ln . There does exist evidence that the effect of disorder is more significant for the vacancy-doped systems, $La_{1-x}TiO_3$, than for $La_{1-x}Sr_xTiO_3$ (14).

In the studies described here, results are presented for the vacancy-doped materials $Ln_{1-x}TiO_3$ where $Ln = Nd$ and Sm . One expects that U/W will increase systematically in the order $Sm > Nd > La$. Electrical transport, thermoelectric power, and specific heat data will be examined in the context outlined above and comparisons will be made to related systems such as $Ln_{1-x}A_xTiO_3$ and the previously studied vacancy-doped system, $La_{1-x}TiO_3$.

EXPERIMENTAL

Sample Preparation of $Nd_{1-x}TiO_3$ and $Sm_{1-x}TiO_3$

Samples were prepared by solid state reaction using the scheme below:



The relevant amounts of Nd_2O_3 (Research Chemicals, 99.99%), Sm_2O_3 (Rhone Poulenc, 99.99%), TiO_2 (Fisher Scientific, 99.9%), and Ti_2O_3 (Cerac, 99.9%) in the form of fine powders were weighed, ground under acetone in a mortar and pestle, and pressed into pellets. The weight of Ti_2O_3 was adjusted for the measured oxygen content of this material, which was checked by thermogravimetric analysis (TGA). The pellets were placed in a molybdenum crucible and the crucible was sealed by welding under purified argon gas. The crucibles were heated in an induction furnace at $1400^\circ C$ for several hours and the temperature was measured to $\pm 50^\circ C$ by an optical pyrometer. Phase purity was monitored by X-ray powder diffraction.

X-Ray Powder Diffraction

A Guinier-Hägg camera (IRDAB Model XDC700) using $CuK\alpha_1$ radiation was used to monitor phase purity and to determine the unit cell parameters with the aid of an internal standard of high-purity silicon powder. The information on the films was converted to a digital file by means of a KEJ instruments LS20 line scanner. The programs SCANPI and LSUDF were used to extract accurate d spacings and to refine the unit cell constants, respectively.

Thermogravimetric Analysis

The samples were analyzed for oxygen content by the oxidative weight gain to $Ln_2Ti_2O_7$ and TiO_2 in flowing air at $1000^\circ C$ with a Netzch STA 409 thermal analyzer.

Electrical Resistivity

Measurements were made by the four-probe van der Pauw method (16) on well-sintered-polycrystalline pellets over the temperature range $\sim 5-300$ K. Ohmic contacts were made by silver paste.

Heat Capacity

The specific heats were measured using an adiabatic heat pulse method in which the sample temperature, T_1 , is monitored for a predefined period of time, t_1 (seconds), after which a heat pulse of known power, P (typically in μW), is applied for t_0 seconds. After a decay period, t_2 (seconds), to allow for internal thermal equilibration of the sample, the temperature is monitored again. The heat capacity, C , is then obtained from the relationship,

$$C = \lim_{\Delta T \rightarrow 0} \left(\frac{Pt_0}{\Delta T} \right),$$

where t_0 is the duration of the heat pulse and ΔT is the temperature difference before (T_1) and after (T_2) the heat pulse is applied. The apparatus consisted of an Oxford Instruments Heliox insert, which is equipped with a sorption pumped 3He refrigerator capable of reaching temperatures below 1 K. An Oxford Instruments ITC503 temperature controller was used for temperature monitoring and variation. The sample was mounted on a sapphire plate affixed to the Heliox insert. A RuO_2 temperature sensor and strain gauge heater were attached to the sapphire plate. The measurements were carried out on polycrystalline samples, which exhibited metallic or near metallic behavior. Typical sample sizes varied from $\sim 125-200$ mg and were ~ 1.5 to 2.0-mm thick.

Thermopower

Seebeck coefficient measurements were carried out using an apparatus constructed locally. A sample in the shape of a block or a disc with flat ends was mounted between two copper heads, A and B, which are in thermal contact with a copper base, C, which is in turn connected to the cold stage of a CTI Model 21C closed cycle refrigerator. Both heads A and B and block C are heated and controlled independently by Lakeshore Model 321 autotuning silicon diode temperature controllers. The thermal gradient, ΔT , across the sample was measured by two chromel vs Au-(0.07% Fe) thermocouples attached directly to the sample via silver paste. The Seebeck voltage, E_S , was measured from two copper wires attached to the sample with silver paste at the same positions as the thermocouples using a Keithley Model 2000 digital multimeter and scanner. The

entire system is controlled with a standard RS232 interface and a 486-66 MHz PC.

The procedure for measuring the Seebeck coefficient, S , involves equilibration of block C at a given temperature slightly below the target temperature and creation of a gradient across the sample by controlling the temperature of head A at T_1 and varying the temperature of head B over the range $T_1 \pm 5$ K in 1 K steps. For each step ΔT and E_S are measured several times for statistical averaging. The Seebeck coefficient, S' , is extracted at each temperature from the slope of the averaged E_S versus the averaged ΔT . The absolute value of the sample is obtained by subtracting the contributions of the silver paste and the copper wires, i.e., $S = S' - S_{Ag} - S_{Cu}$. The system just described was checked against a sample of CePd₃ measured independently at Cornell University courtesy of C. Jones and F. DiSalvo.

RESULTS AND DISCUSSION

Sample Characterization

Phase purity was determined by indexation of the X-ray powder diffraction patterns. Typically, all observable lines (20–35) could be indexed on either a $Pnma$ or $Pban$ unit cell. The derived unit cell constants and volumes are shown in Table 1. In Table 2 the results from the oxidative weight gain experiments are shown. The agreement between the observed and expected values confirms that the sample compositions are generally within range ± 0.01 of the nominal x value.

Resistivity

$Nd_{1-x}TiO_3$. Resistivity data for $Nd_{1-x}TiO_3$, $x = 0.00, 0.05, 0.10, 0.12, 0.15, 0.17, 0.20, 0.25,$ and 0.30 , are shown in

TABLE 1
Unit Cell Constants for $Nd_{1-x}TiO_3$ and $Sm_{1-x}TiO_3$
in $Pnma$ and $Pban$

Compound	a (Å)	b (Å)	c (Å)	V (Å ³)	Space group
$NdTiO_3$	5.6512(5)	7.7927(8)	5.5228(5)	243.22(3)	$Pnma$
$Nd_{0.95}TiO_3$	5.5920(5)	7.7983(8)	5.5059(4)	240.10(3)	$Pnma$
$Nd_{0.90}TiO_3$	5.5508(3)	7.7958(5)	5.4880(3)	237.48(2)	$Pnma$
$Nd_{0.85}TiO_3$	5.5207(5)	7.7804(7)	5.4800(4)	235.37(2)	$Pnma$
$Nd_{0.83}TiO_3$	5.5114(7)	7.7752(10)	5.4780(5)	234.75(3)	$Pnma$
$Nd_{0.80}TiO_3$	5.471(1)	7.7448(6)	5.479(1)	232.18(4)	$Pnma$
$Nd_{0.75}TiO_3$	5.4530(9)	5.4548(7)	7.7629(11)	230.91(4)	$Pban$
$Nd_{0.70}TiO_3$	5.4410(4)	5.4444(1)	7.7357(8)	229.15(6)	$Pban$
$Nd_{0.67}TiO_3$	5.4373(5)	5.4373(5)	7.6974(7)	227.56(4)	$I4/mmm$
$SmTiO_3$	5.6671(5)	7.7314(6)	5.4623(3)	239.25(2)	$Pnma$
$Sm_{0.95}TiO_3$	5.6154(6)	7.7416(6)	5.4542(4)	237.11(3)	$Pnma$
$Sm_{0.90}TiO_3$	5.5774(7)	7.7450(7)	5.4464(6)	235.27(3)	$Pnma$
$Sm_{0.87}TiO_3$	5.5496(7)	7.7442(8)	5.4355(6)	233.43(3)	$Pnma$
$Sm_{0.85}TiO_3$	5.5318(5)	7.7454(10)	5.4376(8)	232.98(4)	$Pnma$
$Sm_{0.83}TiO_3$	5.5176(2)	7.7345(3)	5.4294(2)	231.70(1)	$Pnma$

TABLE 2
Thermogravimetric Oxidative Weight Gain Results
for $Nd_{1-x}TiO_3$ and $Sm_{1-x}TiO_3$

Compound	Weight gain (expected) %	Weight gain (observed) %
$NdTiO_3$	3.33	3.33
$Nd_{0.95}TiO_3$	2.92	2.92
$Nd_{0.90}TiO_3$	2.48	2.38
$Nd_{0.85}TiO_3$	2.01	1.99
$Nd_{0.83}TiO_3$	1.83	1.82
$Nd_{0.80}TiO_3$	1.51	1.42
$Nd_{0.75}TiO_3$	0.97	0.91
$Nd_{0.70}TiO_3$	0.41	0.41
$SmTiO_3$	3.25	3.13
$Sm_{0.95}TiO_3$	2.85	2.78
$Sm_{0.90}TiO_3$	2.42	2.78
$Sm_{0.87}TiO_3$	2.15	1.98
$Sm_{0.85}TiO_3$	1.97	2.00
$Sm_{0.83}TiO_3$	1.78	1.73

Fig. 2. Clearly, the data span 6 to 7 orders of magnitude and the two expected MITs are evident. For example, the curves for $x = 0.30$ and 0.25 are representative of the electron-doped CTI regime. Data for $x = 0.33$ ($Nd_{2/3}TiO_3$) are not shown. This sample has a room temperature resistivity of $>10^6 \Omega\text{-cm}$ and the data would be well off the scale of the figure. Insulating behavior also pertains for $x = 0.00$ and 0.05 , in the MHI hole-doped regime. The samples of intermediate composition all have values in the range 10^{-2} – $10^{-4} \Omega\text{-cm}$ and can be classified as poor metals.

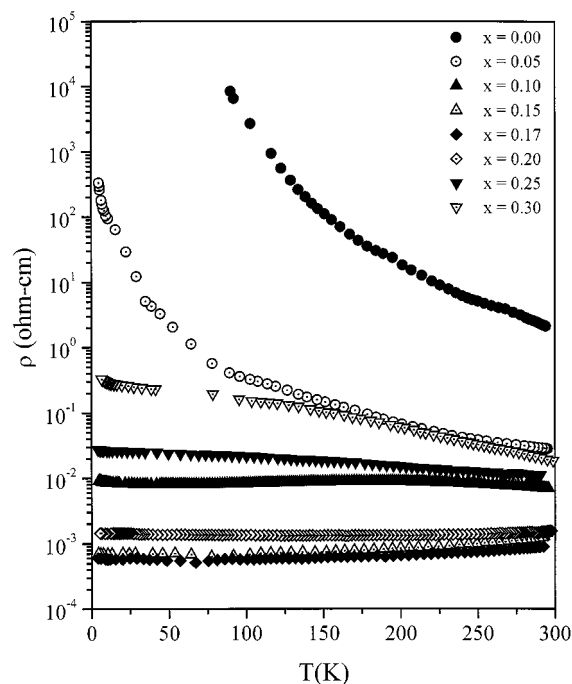


FIG. 2. Resistivity vs temperature data for the $Nd_{1-x}TiO_3$ series.

Beginning from the CTI end, electron doping results in a MIT commencing between $x = 0.25$ and $x = 0.20$. Assuming that $n = [\text{Ti}^{3+}]$ in the solid solution, this places $n_c(1)$ at about $5 \times 10^{21} \text{ cm}^{-3}$. This is a significantly higher value than observed for the much studied $\text{La}_{1-x}\text{Sr}_x\text{TiO}_3$ series where $n_c(1) < 8 \times 10^{20} \text{ cm}^{-3}$ (17). The low value in the latter can be traced to the anomalously high dielectric constant for SrTiO_3 , as according to Mott (9),

$$a_0 [n_c(1)]^{1/3} \sim 0.25, \quad [1]$$

where $a_0 = a_H \kappa(m^*/m_0)^{-1}$ and a_H is the Bohr radius, κ the dielectric constant, and m^*/m_0 the effective mass ratio. The $n_c(1)$ value observed for $\text{Nd}_{1-x}\text{TiO}_3$ falls into the range observed for several other electron-doped transition metal oxides with more normal dielectric constants, $4-6 \times 10^{-21} \text{ cm}^{-3}$ (18). A more detailed look at the behavior in the CTI regime is afforded by Fig. 3 in which results for $x = 0.30$ are examined in detail. An attempt was made to fit the data below 50 K to either an activated or variable range hopping model (10). Analysis in terms of a simple activated hopping was not successful but plots of $\log \sigma T^{1/2}$ versus $T^{-1/4}$ resulted in a good linear region, extending from about 6 to ~ 60 K. Above 60 K perhaps several mechanisms contribute, rendering a more detailed analysis difficult. The resistivity for $x = 0.25$, Fig. 2, which is closer to $n_c(1)$, shows an unusual, almost linear, increase with decreasing temperature, which does not conform to any simple transport mechanism.

On the metallic side of $n_c(1)$, data for $x = 0.20, 0.17, 0.15$, and 0.12 are shown in Fig. 4a. Fits to the Fermi-liquid expression,

$$\rho = \rho_0 + AT^2 \quad [2]$$

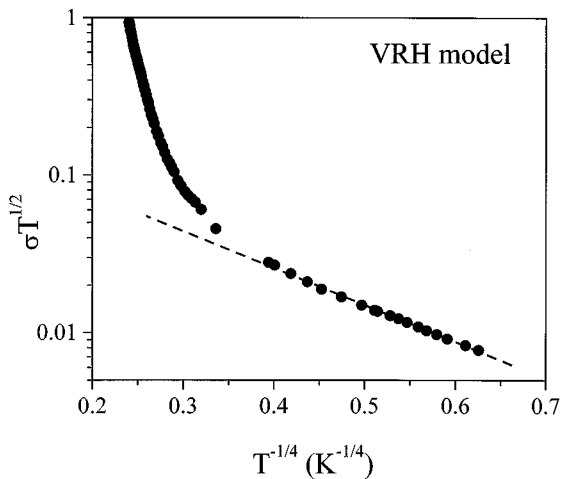


FIG. 3. The analysis of the data for $\text{Nd}_{0.70}\text{TiO}_3$ in terms of a variable range hopping (VRH) model.

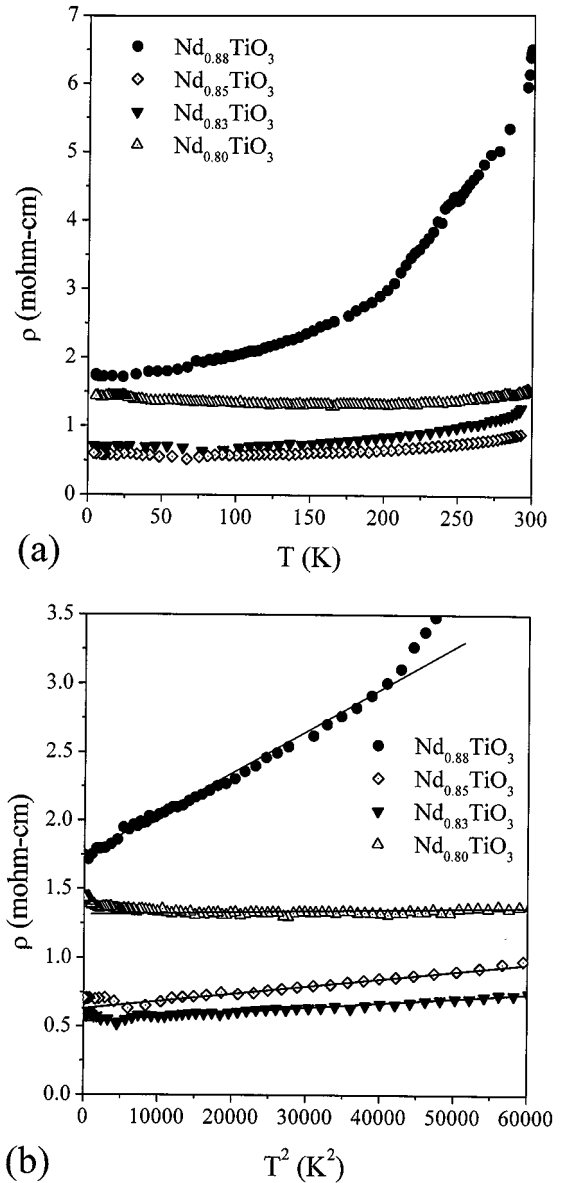


FIG. 4. (a) Resistivity vs temperature data for metallic members of the $\text{Nd}_{1-x}\text{TiO}_3$ series, $x = 0.12, 0.15, 0.17$, and 0.20 . (b) Fermi-liquid behavior for the samples shown in Fig. 4a. The lines are fits to Eq. [2].

appear in Fig. 4b, where the T^2 behavior seems to hold up to about $T = 250$ K for the samples studied. Values of the coefficient, A , extracted from the plots are shown in Fig. 5, compared with values for similar carrier concentrations in the $\text{La}_{1-x}\text{TiO}_3$ and $\text{La}_{1-x}\text{Sr}_x\text{TiO}_3$ series. The values of the A coefficients are often taken as a measure of the extent of electron correlation in the metallic state and are expected to increase as n approaches $n_c(2)$ and to increase for constant n as the importance of correlation increases. These expectations are clearly met here as the A values for the Nd vacancy-doped system are greater by

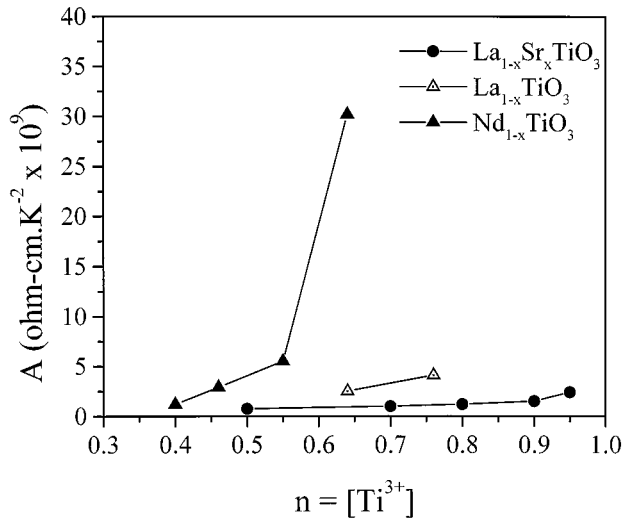


FIG. 5. Values of the Fermi-liquid parameter, A , as a function of n (carrier density or $[\text{Ti}^{3+}]$) for the $\text{Nd}_{1-x}\text{TiO}_3$, $\text{La}_{1-x}\text{TiO}_3$, and $\text{La}_{1-x}\text{Sr}_x\text{TiO}_3$ series.

significant factors for the same nominal n . Indeed, A for the $x = 0.12$ composition, $3.0 \times 10^{-8} \Omega\text{-cm K}^{-2}$, is about 10 times larger than any value reported previously for a titanate material and is at the level of the so-called heavy fermions (19). This pronounced increase in electron correlation as the MIT is approached from the metallic side should also be reflected in the heat capacity data in the form of a significant electron mass enhancement and data to support this point will be presented in the next section.

The $x = 0.10$ sample shows singular behavior, Fig. 6, with an increasing resistivity from 300 K to a broad maximum at

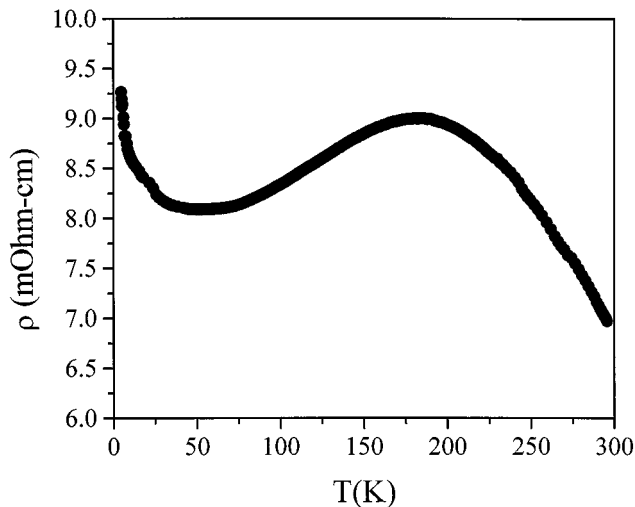


FIG. 6. Kondo or valence-fluctuating behavior of the resistivity for $\text{Nd}_{0.90}\text{TiO}_3$.

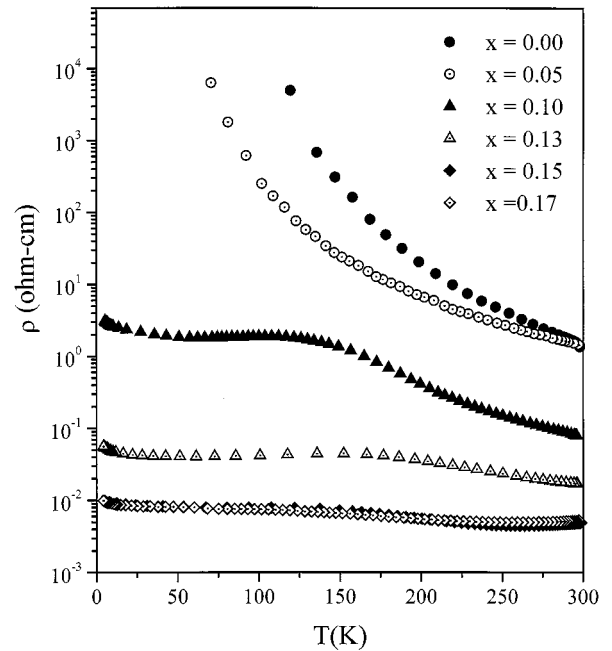


FIG. 7. Resistivity vs temperature data for the $\text{Sm}_{1-x}\text{TiO}_3$ series.

175 K followed by a decrease to a shallow minimum near 50 K and another upturn at the lowest temperatures. Nonetheless, even near 4.2 K, the resistivity values do not exceed $10^{-2} \Omega\text{-cm}$. This is reproducible for other samples with the same nominal x . As similar curves are found for the $\text{Sm}_{1-x}\text{TiO}_3$ series, more detailed comments will be deferred to the next section.

For the semiconducting compositions, $x = 0.00$ and 0.05 , a simple Arrhenius law analysis of the high-temperature data yields activation energies of 0.032(1) and 0.12(1) eV, respectively. The latter value is in excellent agreement with other reports (20). Both of these compositions are antiferromagnetic with $T_N = 100$ K ($x \sim 0.00$) and 75 K ($x = 0.05$) (21). The $x = 0.10$ material shows no magnetic order associated with the Ti sublattice.

$\text{Sm}_{1-x}\text{TiO}_3$. Figure 7 shows the overall result for this series, which extends only from $x = 0.00$ to $x = 0.17$. Again, the data span several orders of magnitude. For the semiconductors, $x = 0.00$ and 0.05 , an Arrhenius law fit gives activation energies of 0.06 and 0.08 eV, respectively. When the vacancy levels are increased to near a nominal $x = 0.10$, the resistivity drops by a factor of 10^3 – 10^4 , especially at low temperatures and the detailed behavior becomes extremely sensitive to very small changes in composition. Figure 8a shows data for three samples (A, B, and C) near $x = 0.10$ and among them there is a variation of about 10^3 in the resistivity values below 100 K. For larger x , $0.13 < x < 0.17$, Fig. 8b, there is much less variation. Note that all the

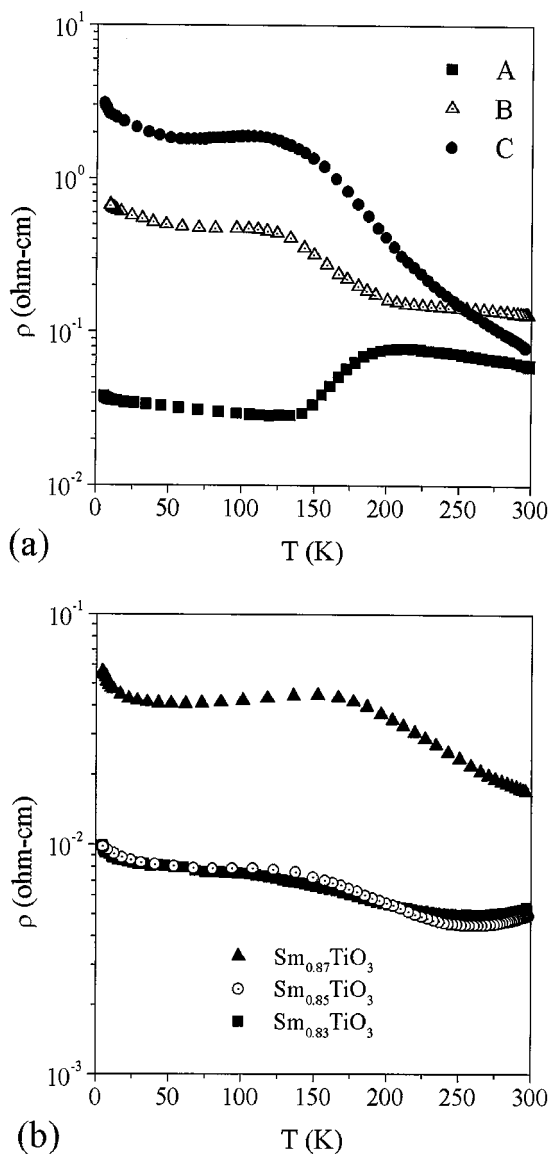


FIG. 8. (a) Resistivity vs temperature for three samples (A, B, and C) of nominal composition $\text{Sm}_{0.90}\text{TiO}_3$. (b) Resistivity vs temperature for $\text{Sm}_{1-x}\text{TiO}_3$, $x = 0.13, 0.15,$ and 0.17 , a linear basis.

samples in the range $0.10 < x < 0.17$ have common features, which include (1) no evidence for an activated resistivity except, possibly, below 10 K, (2) a prominent maximum between 100 and 200 K, (3) at least one minimum between 30 and 100 K (the $x = 0.15$ and 0.17 materials have a second shallow minimum near 260 K), and (4) no evidence for typical Fermi-liquid behavior in the form of a T^2 dependence within the temperature range investigated. Recall that $\text{Nd}_{0.90}\text{TiO}_3$ ($x = 0.10$) shows similar behavior, but for $\text{Nd}_{1-x}\text{TiO}_3$ with larger x values, standard Fermi-liquid properties are seen. Similar non-Fermi-liquid behavior, as exhibited by the cation vacancy doped titanates, is seen in the related $\text{Sm}_{1-x}\text{Ca}_x\text{TiO}_3$ system for which a MIT occurs

between $x = 0.20$ and $x = 0.24$, $[\text{Ti}^{3+}] = 0.80$ to 0.76 (22). For corresponding $[\text{Ti}^{3+}]$ levels in $\text{Sm}_{1-x}\text{TiO}_3$, $x = 0.07$ – 0.08 , an insulating state still exists. While the barely metallic $\text{Sm}_{0.76}\text{Ca}_{0.24}\text{TiO}_3$ exhibits a weak maximum above 200 K, the resistivity drops rapidly and reaches values of 10^{-4} $\Omega\text{-cm}$ near 4 K. Similar behavior is exhibited by $\text{Y}_{0.61}\text{Ca}_{0.39}\text{TiO}_3$ (23). These results for the Sm–Ca and Y–Ca titanates have been interpreted as evidence for the intermediate Kondo-like state predicted by theory (12).

The ρ versus T curves for the conducting members of the $\text{Sm}_{1-x}\text{TiO}_3$ series and $\text{Nd}_{0.90}\text{TiO}_3$ show the resistivity maximum in a similar temperature range but also new features, an additional minimum below the maximum and the upturn at the lowest temperatures. These results resemble those commonly found for the so-called valence-fluctuating compounds, CeRhSb and CeNiSn being examples (24, 25). The Ce valences are $\text{Ce}^{3+}(4f^1)$ and $\text{Ce}^{4+}(4f^0)$. In these materials and the related Kondo systems, an unusual electronic ground state exists involving hybridization of localized $4f$ states, associated with $\text{Ce}^{3+}(4f^1)$, and the conduction electrons. Applying this picture to the titanates, which involve formally $\text{Ti}^{3+}(3d^1)$ and $\text{Ti}^{4+}(3d^0)$, would require postulation of a co-existence of localized and delocalized $3d^1$ electrons associated with the Ti^{3+} sites in some sort of highly hybridized state. In addition, the valence-fluctuating systems, such as those based on Ce intermetallics, usually develop a very narrow gap at the Fermi level of the order of a few K, leading to the upturn in the resistivity at the lowest temperatures. For the titanates, Fig. 9, the data below about 10 K are fitted with an Arrhenius type analysis, yielding activation energies of the order of 0.6 to 0.9 K, remarkably low values, and an order of magnitude smaller than those for the Ce intermetallics. Thus, the vacancy-doped titanates, $\text{Nd}_{0.90}\text{TiO}_3$ and $\text{Sm}_{1-x}\text{TiO}_3$ for $x \geq 0.10$, show complex electrical transport not seen before in other doped titanates nor, indeed, to our knowledge, in other MHI materials near or at the MIT. These novel effects appear to be driven by the enhanced correlation levels present in the vacancy-doped materials. Further information on electron correlation can be obtained from heat capacity measurements.

Heat Capacity

Heat capacity data for the most conducting members of the $\text{Nd}_{1-x}\text{TiO}_3$ and $\text{Sm}_{1-x}\text{TiO}_3$ series are presented in Figs. 10a and 11a, respectively. The most striking feature, initially, is the presence of large maxima near or below 1 K. These features are generally sharp and suggest a phase transition that can be assigned to the magnetic ordering of the Ln^{3+} sublattice moments. Similar ordering temperatures are reported for the isostructural and related LnAlO_3 and LnCrO_3 perovskites (26). The presence of such strong maxima at low temperatures complicates the analysis of the

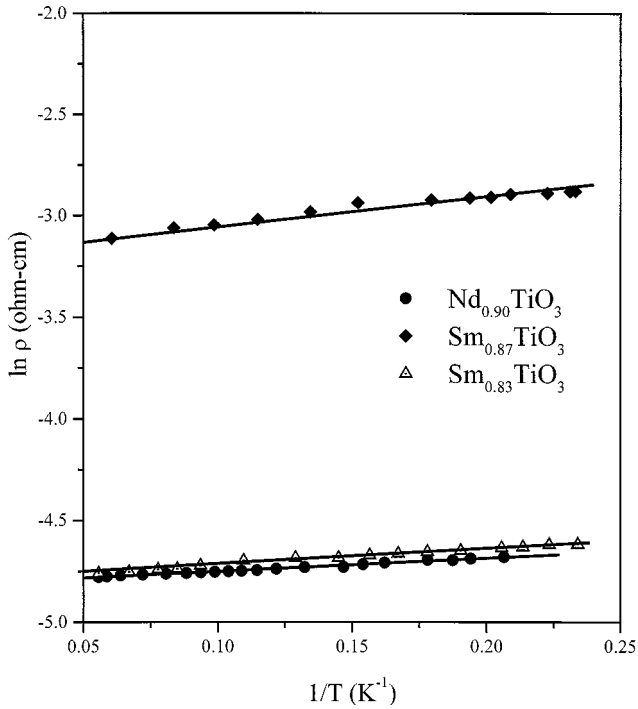


FIG. 9. Arrhenius plots for the very low temperature resistivity data for $\text{Nd}_{0.90}\text{TiO}_3$, $\text{Sm}_{0.87}\text{TiO}_3$, and $\text{Sm}_{0.83}\text{TiO}_3$ showing evidence for a gap of $E_a < 1$ K.

heat capacity data and the search for carrier mass enhancement. It is usual to assume that, apart from magnetic contributions, the heat capacity at low temperatures will be comprised of electronic and lattice contributions according to

$$C = \gamma T + \beta T^3. \quad [3]$$

Indeed, plots of C/T versus T^2 , Figs. 10b and 11b, show a well-defined linear region above about 6 K. It can be assumed that the magnetic contribution from the anomalies below 1 K is negligible in this range. Within the Fermi-gas approximation γ is proportional to the density of states at E_F and can further be related to the carrier effective mass, m^* , as

$$\gamma = C_h m^* n^{-2/3}, \quad [4]$$

where C_h is a constant and n is the carrier density.

The γ values extracted from the linear regions of these plots are collected in Table 3 and values for $\text{Nd}_{1-x}\text{TiO}_3$ are displayed in Fig. 12a where a comparison is made with two closely related series, $\text{La}_{1-x}\text{Sr}_x\text{TiO}_3$ and $\text{La}_{1-x}\text{TiO}_3$. Within the Fermi-liquid model, γ is directly proportional to the carrier effective mass and two expected trends are clearly evident. First, for the same n or $[\text{Ti}^{3+}]$, γ increases in the order $\text{La}_{1-x}\text{Sr}_x\text{TiO}_3 < \text{La}_{1-x}\text{TiO}_3 < \text{Nd}_{1-x}\text{TiO}_3$,

$\text{Sm}_{1-x}\text{TiO}_3$, which follows the order of expected increase in the correlation parameter, U/W . Secondly, γ also increases sharply as $n_c(2)$ is approached, consistent with most current ideas for the MIT. Additionally, the actual γ values are the largest yet observed for oxide titanates, reaching a level of $\sim 50 \text{ mJ mol}^{-1} \text{ K}^{-2}$ for $\text{Nd}_{0.85}\text{TiO}_3$ and $\text{Sm}_{0.87}\text{TiO}_3$. For the $\text{La}_{1-x}\text{Sr}_x\text{TiO}_3$, $\text{La}_{1-x}\text{TiO}_3$, and $\text{Y}_{1-x}\text{Ca}_x\text{TiO}_3$ series the maximum observed γ 's are 17, 13, and 13 $\text{mJ mol}^{-1} \text{ K}^{-2}$ (15, 16). As well, the superconductor LiTi_2O_4 shows a value of about 20 $\text{mJ mol}^{-1} \text{ K}^{-2}$ (27). Also remarkable is that a linear C/T versus T^2 correlation is seen for the $\text{Sm}_{1-x}\text{TiO}_3$ materials in spite of the non-Fermi-liquid behavior at low temperatures. This suggests the presence of some finite concentration of correlated, itinerant electrons in the

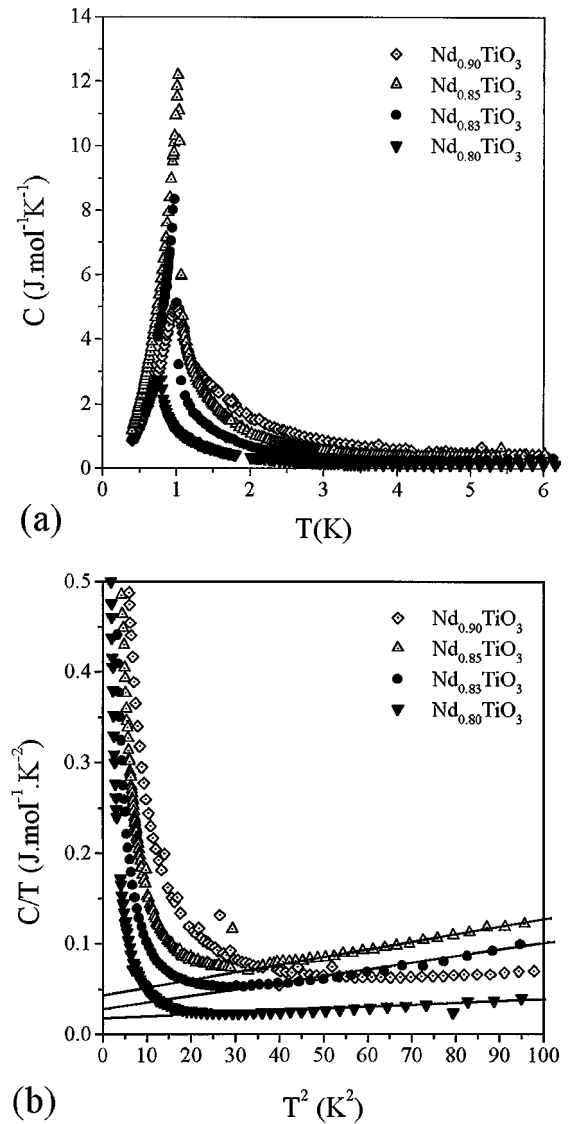


FIG. 10. (a) Heat capacity vs temperature for $\text{Nd}_{1-x}\text{TiO}_3$, $x = 0.00, 0.10, 0.15, 0.17, \text{ and } 0.20$. (b) The data of samples shown in Fig. 10a fitted to Eq. [3].

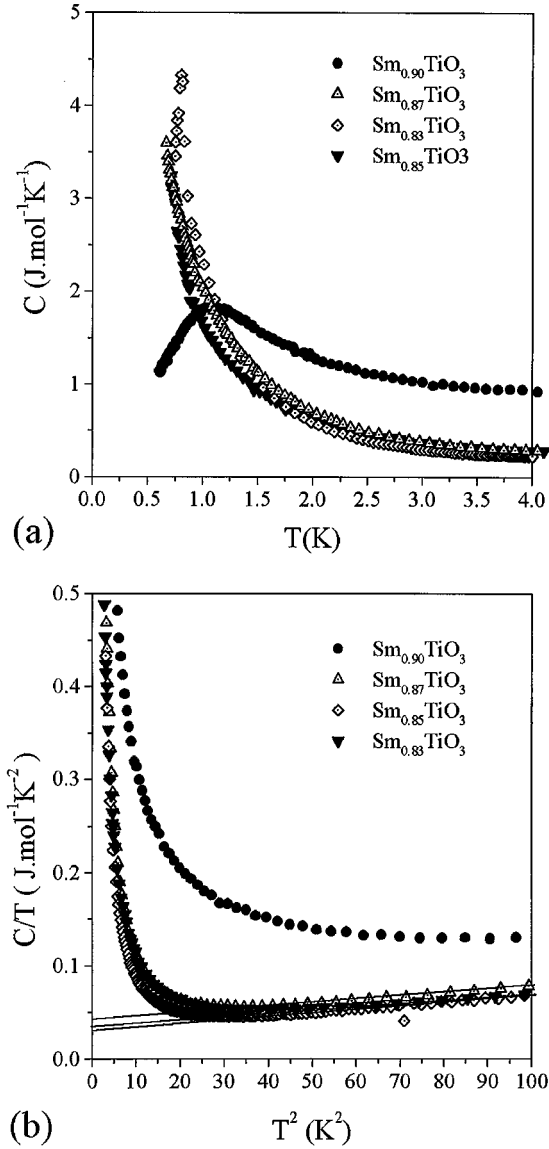


FIG. 11. (a) Heat capacity vs temperature data for $\text{Sm}_{1-x}\text{TiO}_3$, $x = 0.10, 0.13, 0.15,$ and 0.17 . (b) The data of samples shown in Fig. 11a fitted to Eq. [3].

$\text{Sm}_{1-x}\text{TiO}_3$ system and is possible evidence for the co-existence with localized $3d$ electrons, perhaps in some sort of Kondo-like state, as mentioned earlier. Note also that

the γ values for the Kondo-like compositions (Nd , $x = 0.10, \text{Sm}$, $x = 0.13, 0.15,$ and 0.17) are all very similar, $\sim 20\text{--}30 \text{ mJ mol}^{-1} \text{K}^{-2}$.

It is possible that even larger γ or m^*/m_0 values can be reached in the $\text{Nd}_{1-x}\text{TiO}_3$ materials. For example, Kadowaki and Woods have pointed out that an empirical correlation exists between the Fermi-liquid coefficient, A , and γ , to wit (19):

$$A/\gamma^2 = \text{const.} \quad [5]$$

Figure 12b shows this relationship for the $\text{Nd}_{1-x}\text{TiO}_3$ series. Unfortunately, a measured γ is not yet available for the most interesting case, $x = 0.12$, but a linear correlation clearly holds for the other three members and extrapolation suggests the remarkable value of $180 \text{ mJ mol}^{-1} \text{K}^{-2}$. This is in the range seen only in heavy fermion materials and among metallic oxides only LiV_2O_4 with $\gamma = 420 \text{ mJ mol}^{-1} \text{K}^{-2}$ shows a higher value (28).

To summarize the situation so far, both cation vacancy doped systems studied here, $\text{Nd}_{1-x}\text{TiO}_3$ and $\text{Sm}_{1-x}\text{TiO}_3$, show effects of enhanced electron correlation relative to titanate materials studied previously. Qualitatively, this can be understood in terms of a correlation parameter, U/W , and expected decreases in the bandwidth, W , as the Ln^{3+} substitutions occur in the direction La to Nd to Sm . Correlation effects manifest themselves differently in the two systems. For the Nd -based materials, Fermi-liquid behavior occurs for low carrier densities just beyond $n_c(1)$ and increasing correlation drives the carrier mass to unprecedented values just below $n_c(2)$. Also near the MIT at $n_c(2)$ a non-Fermi-liquid state is found that resembles a Kondo or valence-fluctuating state. For the Sm -based materials, correlation effects are so dominant that a Fermi-liquid regime is never realized but conducting phases with resistivities in the range of $10^{-3} \Omega\text{-cm}$ exist, which also resemble valence-fluctuating or Kondo-type systems. We now turn to a discussion of the thermopower measurements, which can provide further insight into these unusual materials.

Thermopower

Under favorable conditions, measurement of the thermoelectric power or, more properly, the Seebeck coefficient,

TABLE 3
Values of γ and β Extracted from Fits of Eq. [3] to the Data of Figs. 12b and 13b

$\text{Nd}_{1-x}\text{TiO}_3$			$\text{Sm}_{1-x}\text{TiO}_3$		
x	γ ($\text{mJ mol}^{-1} \text{K}^{-2}$)	β ($\text{mJ mol}^{-1} \text{K}^{-4}$)	x	γ ($\text{mJ mol}^{-1} \text{K}^{-2}$)	β ($\text{mJ mol}^{-1} \text{K}^{-4}$)
0.10	20.4(8)	0.470(6)	0.13	34.9(2)	0.44(3)
0.15	42.4(7)	0.840(6)	0.15	23.3(5)	0.445(8)
0.17	23.0(2)	0.78(3)	0.17	22.8(7)	0.402(6)
0.20	11.3(9)	0.300(5)			

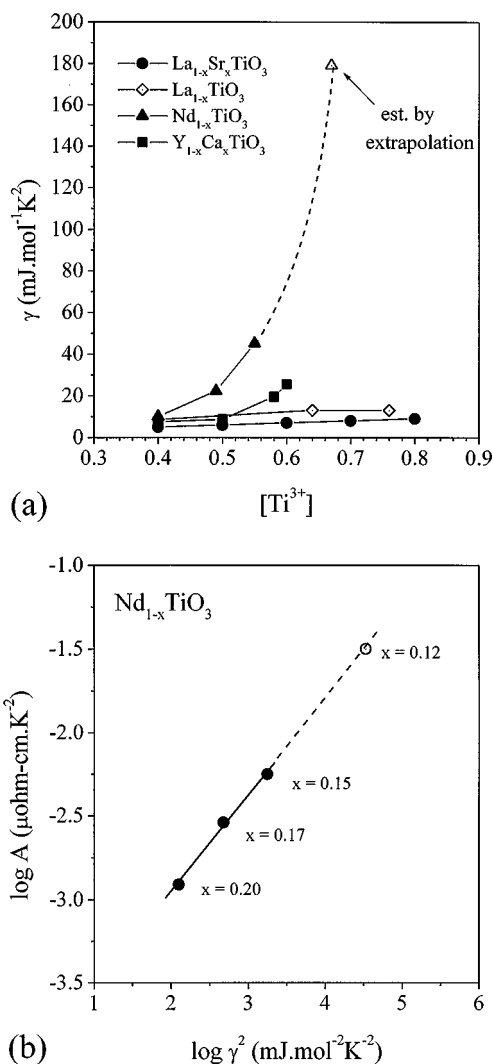


FIG. 12. (a) Heat capacity γ values for $\text{Nd}_{1-x}\text{TiO}_3$ compared with those for related titanate systems. (b) A Kadowaki-Woods-type correlation for $\text{Nd}_{1-x}\text{TiO}_3$ showing an extrapolation for $x = 0.12$, which would give $\gamma \approx 180 \text{ mJ mol}^{-2} \text{ K}^{-2}$.

S , can provide information on the details of the charge conduction mechanism. The sign of S is normally correlated with that of the dominant charge carrier and the magnitude and temperature dependence of S are quite distinct for several idealized conduction mechanisms. For example, $S \sim$ a few $\mu\text{V}/\text{K}$ and a T^1 dependence is expected for metallic conduction, $S \sim 10^2 \mu\text{V}/\text{K}$ and a T^{-1} law holds for conventional band semiconductors, while a T^0 dependence is found for small polaron or “hopping” semiconductors and a $T^{1/2}$ behavior for variable range hopping in three dimensions (29). Seebeck effect measurements are fairly rare for titanate materials; the only systematic study available is that for the $\text{La}_{1-x}\text{Sr}_x\text{TiO}_3$ solid solution (30), which has also been the subject of recent theoretical work (31). The

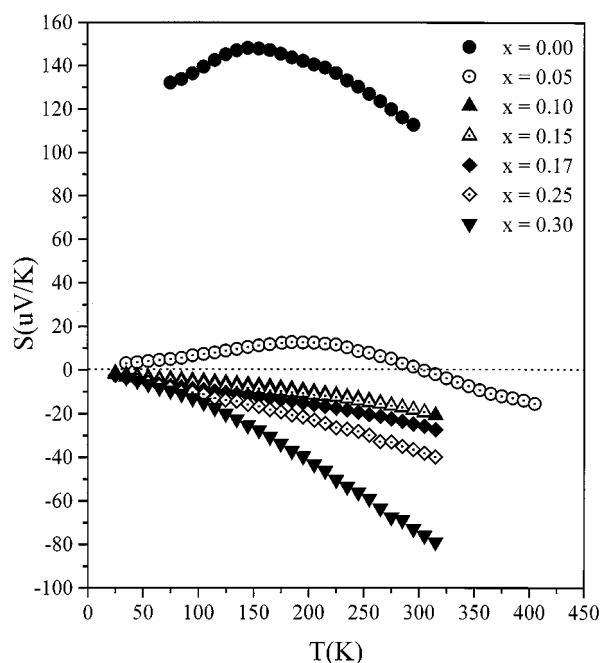


FIG. 13. Seebeck coefficient vs temperature for the $\text{Nd}_{1-x}\text{TiO}_3$ series.

results for $\text{Nd}_{1-x}\text{TiO}_3$ and $\text{Sm}_{1-x}\text{TiO}_3$ are shown in Figs. 13 and 14, respectively. Globally, both systems show a qualitative correlation with the phase diagram of Fig. 1. That is, beginning at the MHI side, p-type semiconducting behavior obtains for small doping levels, $x = 0.0$ and 0.05 , which gives way to n-type metallic compoment between

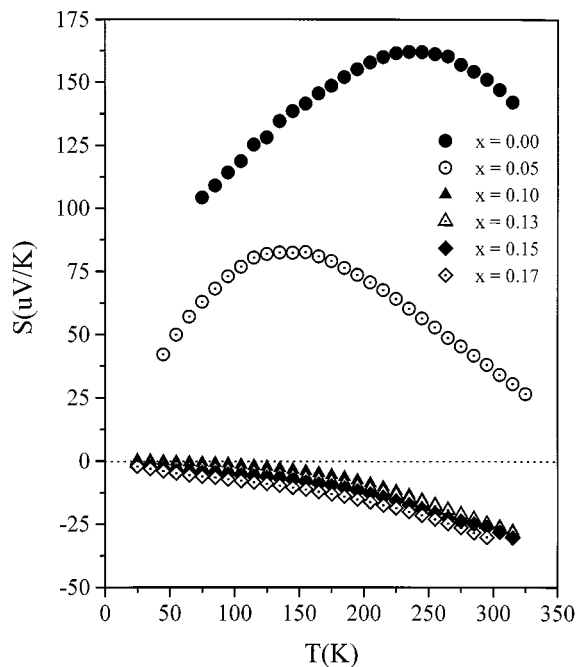


FIG. 14. Seebeck coefficient vs temperature for the $\text{Sm}_{1-x}\text{TiO}_3$ series.

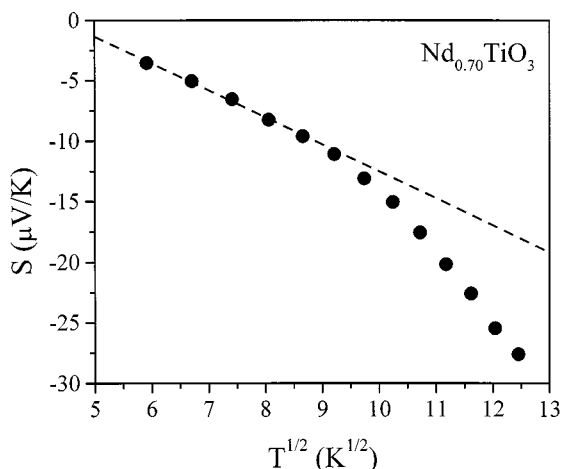


FIG. 15. Evidence for variable range hopping in $\text{Nd}_{0.70}\text{TiO}_3$ in the form of a $T^{1/2}$ dependence for the Seebeck coefficient over the range $35 < T < 70$ K.

$n_c(2)$ and $n_c(1)$, $x \sim 0.10$ to 0.20 , and again to large S values and semiconducting behavior as the CTI state is approached for vacancy-doping levels beyond $n_c(1)$, $x > 0.20$, at least for $\text{Nd}_{1-x}\text{TiO}_3$. It is clear from both figures that for no composition is a T^0 regime realized within the temperature range studied and this suggests that conventional small polaron hopping is not likely to be important until higher temperatures. This is more or less the prediction of the calculations (31). Returning to the p-type regime, the evidence is against a simple, single carrier model given the change of sign observed for $\text{Nd}_{0.95}\text{TiO}_3$ at about 300 K. A similar result has been reported for $\text{Y}_{1-x}\text{Ca}_x\text{TiO}_3$ for $x = 0.39$ and 0.42 (22). There are indications that a sign change could occur for $\text{Sm}_{0.95}\text{TiO}_3$ at higher temperatures. No such sign change with temperature is predicted for the related $\text{La}_{1-x}\text{Sr}_x\text{TiO}_3$ system, which involves a single carrier model for small x (31). The source of the n-type carriers can only be the subject of speculation at present but oxide ion vacancies are a possible origin.

Recall that, in the lightly electron-doped regime for $\text{Nd}_{1-x}\text{TiO}_3$, $x = 0.30$, resistivity data from 6 to ~ 70 K seem to be consistent with a VRH transport mechanism. For three dimensions one would, thus, expect a $T^{1/2}$ dependence of the Seebeck coefficient and evidence for this is seen in Fig. 15 over the range 34 to 70 K, in excellent agreement with the resistivity results (Fig. 3).

Turning to the metallic or quasi-metallic regime for $\text{Nd}_{1-x}\text{TiO}_3$ and $\text{Sm}_{1-x}\text{TiO}_3$, Figs. 13 and 14, one might expect a T^1 dependence to obtain as the temperature approaches 300 K as such behavior was seen for the $\text{La}_{1-x}\text{Sr}_x\text{TiO}_3$ system (29). An unambiguously linear regime is, unfortunately, not observed for any of the samples up to 300 K, the limit of the data. This suggests that the conduction mechanism is more complex for these cation vacancy

doped titanates than that for $\text{La}_{1-x}\text{Sr}_x\text{TiO}_3$ and data at higher temperatures may be needed before a detailed understanding can be obtained.

SUMMARY AND CONCLUSIONS

The perovskite titanate solid solutions, $\text{Nd}_{1-x}\text{TiO}_3$ and $\text{Sm}_{1-x}\text{TiO}_3$, have been shown to exhibit phenomena consistent with very high levels of electronic correlation. For the Nd-based system it is possible to study the entire composition range between a CTI (charge-transfer insulating) state, $x = 0.33$, and an AF-MHI (antiferromagnetic Mott-Hubbard insulating) state, $x = 0.00$. Electron doping of $\text{Nd}_{0.67}\text{TiO}_3$ induces a CTI to correlated metal, Fermi-liquid, transition at $n_c(1) \approx 5 \times 10^{21} \text{ cm}^{-3}$, $x \approx 0.20$, a level similar to those for related transition metal oxides.

Resistivity and specific heat studies show that, with increasing carrier concentration, n , the correlation levels increase sharply, in agreement with theory, as a second metal-insulator transition is approached at $n_c(2) \approx 1.2 \times 10^{22} \text{ cm}^{-3}$, $x \approx 0.10$. Values for the T^2 resistivity coefficient and the heat capacity γ recorded near $n_c(2)$ are the largest yet seen in titanate oxides and approach those found only in the so-called heavy fermion materials. For $\text{Nd}_{0.90}\text{TiO}_3$ a very unusual non-Fermi-liquid conducting state is found that shows properties including resistivity maxima and minima seen in Kondo or valence-fluctuating Ce- or U-based intermetallic compounds. This is qualitatively consistent with existing theory, which predicts that a Kondo-like state will be intermediate between the FL and MHI states. In addition, evidence for a very small gap, $E_g < 1 \text{ eV}$, is seen at the lowest temperatures, which is not predicted by any theory of which we are aware.

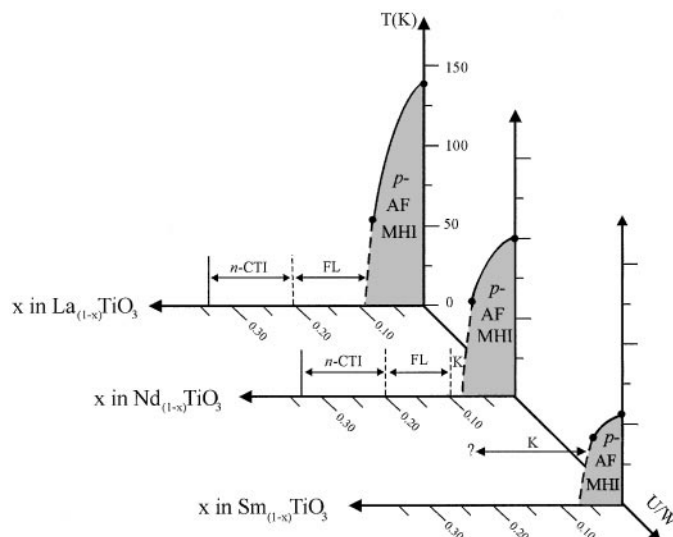


FIG. 16. Electronic phase diagrams for the vacancy-doped $\text{La}_{1-x}\text{TiO}_3$, $\text{Nd}_{1-x}\text{TiO}_3$, and $\text{Sm}_{1-x}\text{TiO}_3$ systems showing the dramatic effect of increasing the correlation coefficient, U/W .

Beginning at the AF-MHI end, $x = 0.00$, hole doping destroys the AF order as $n_c(2)$ is approached. Thermopower data indicate a more complex situation as a p- to n-type crossover is seen near 300 K for $\text{Nd}_{0.95}\text{TiO}_3$.

The effects of electron correlation are even more pronounced in $\text{Sm}_{1-x}\text{TiO}_3$ as only the AF-MHI and Kondo-like states are encountered with no evidence for a Fermi-liquid regime down to $x = 0.17$, the chemical limit for the solid solution.

Finally, in Fig. 16, the above results for the vacancy-doped NdTiO_3 and SmTiO_3 series are compared with those for $\text{La}_{1-x}\text{TiO}_3$, which shows no evidence for the intermediate Kondo or valence-fluctuating state. This figure illustrates the dramatic effect that enhancement of the correlation coefficient, U/W , has on the electronic structure of these titanate systems.

ACKNOWLEDGMENTS

J. E. G. acknowledges support through a Natural Sciences and Engineering Research Council of Canada Research grant. We thank C. Adams and T. Mason for assistance with the heat capacity measurements and B. Collier, J. D. Garrett, A. Dabkowski, and T. Timusk for considerable efforts in the design and construction of the thermopower apparatus.

REFERENCES

- H. J. de Boer and E. J. W. Verwey, *Proc. Phys. Soc. London Ser. A* **49**, 59 (1937).
- N. F. Mott, *Proc. Phys. Soc. London Ser. A* **62**, 416 (1949).
- J. Hubbard, *Proc. R. Soc. London A* **277**, 237 (1964); **281**, 401 (1964).
- J. Zaanen, G. A. Sawatzky, and J. W. Allen, *Phys. Rev. Lett.* **55**, 418 (1985); J. Zaanen and G. Sawatzky, *J. Solid State Chem.* **88**, 8 (1990).
- J. M. Tranquada, J. E. Lorenzo, D. J. Buttrey, and V. Sachan, *Phys. Rev. B* **52**, 3581 (1995).
- Y. Okimoto, T. Katsufuji, Y. Okada, T. Arima, and Y. Tokura, *Phys. Rev. B* **51**, 9581 (1995).
- D. A. Crandles, T. Timusk, J. D. Garrett, and J. E. Greedan, *Phys. Rev. B* **49**, 16207 (1994).
- D. A. MacLean, H. N. Ng, and J. E. Greedan, *J. Solid State Chem.* **30**, 35 (1979).
- N. F. Mott, in "Metal-Insulator Transitions," p. 133, Taylor and Francis, London, 1974.
- P. W. Anderson, *Phys. Rev.* **109**, 1492 (1958); *Commun. Solid State Phys.* **2**, 193 (1970); N. F. Mott, in "Metal-Insulator Transitions," pp. 30–40. Taylor and Francis, London, 1974.
- W. F. Brinkman and T. M. Rice, *Phys. Rev. B* **2**, 4302 (1970).
- X. Y. Zhang, M. J. Rosenberg, and G. Kotliar, *Phys. Rev. Lett.* **70**, 1166 (1993); M. J. Rosenberg, G. Kotliar, and X. Y. Zhang, *Phys. Rev. B* **49**, 10181 (1994).
- M. Imada, A. Fujimori, and Y. Tokura, *Rev. Mod. Phys.* **70**, 1165–1171 (1998).
- M. J. MacEachern, H. Dabkowska, J. D. Garrett, G. Amow, W. Gong, G. Liu, and J. E. Greedan, *Chem. Mater.* **6**, 2092 (1994).
- G. Amow, *Ph.D. thesis*, McMaster University, 1999.
- L. J. van der Pauw, *Philips Res. Repts.* **13**, 1 (1958).
- P. A. Cox, in "Transition Metal Oxides: An Introduction to Their Electronic Structure and Properties," p. 195. Clarendon Oxford, 1992.
- K. Kadowaki and S. B. Woods, *Solid State Commun.* **58**, 507 (1986).
- H. L. Ju, J. L. Eylem, B. Peng, B. Eichhorn, and R. L. Greene, *Phys. Rev. B* **49**, 13335 (1994).
- G. Amow, and J. E. Greedan, *J. Solid State Chem.* **121**, 443 (1996); G. Amow, J. E. Greedan, and C. Ritter, *J. Solid State Chem.* **141**, 262 (1998).
- T. Katsufuji, Y. Taguchi, and Y. Tokura, *Phys. Rev. B* **56**, 10145 (1997).
- F. Iga, Y. Nishihara, J. Sakurai, and M. Ishikawa, *Physica B* **237–238**, 14 (1997).
- S. K. Malik and D. T. Adroja, *Phys. Rev. B* **43**, 6277 (1991).
- T. Takabatake, F. Teshima, H. Fujii, S. Nishigori, T. Suzuki, T. Fujita, Y. Yamaguchi, J. Sakurai, and D. Jaccard, *Phys. Rev. B* **41**, 9607 (1990).
- J. B. Goodenough and J. M. Longo, in "Crystallographic and Magnetic Properties of Perovskites and Perovskite-Related Compounds," pp. 227 and 239. Landolt-Bornstein **III/4a**, Springer-Verlag, Berlin, Heidelberg, 1970.
- K. Kumagai, T. Suzuki, Y. Taguchi, Y. Okada, Y. Fujishima, and Y. Tokura, *Phys. Rev. B* **48**, 7636 (1993).
- R. W. McCallum, D. C. Johnston, C. A. Luengo, and M. B. Maple, *J. Low Temp. Phys.* **25**, 177 (1976).
- S. Kondo, D. C. Johnston, C. A. Swenson, F. Bora, A. V. Mahajan, L. L. Miller, T. Gu, A. I. Goldman, M. B. Maple, D. A. Gajewski, E. J. Freeman, N. R. Dilley, R. P. Dickey, J. Merrin, K. Kojima, G. M. Luke, Y. J. Uemura, O. Chmaisson, and J. D. Jorgensen, *Phys. Rev. Lett.* **70**, 3729 (1997). D. C. Johnston, C. A. Swenson, and S. Kondo, *Phys. Rev. B* **59**, 2627 (1999).
- P. M. Chaikin, in "Organic Superconductivity," (V. Z. Kresin and W. A. Little, Eds.), pp. 101–115. Plenum, New York, 1990.
- R. Moos, A. Gnudi, and K. H. Hardtl, *J. Appl. Phys.* **78**, 5042 (1995).
- G. Palsson and G. Kotliar, *Phys. Rev. Lett.* **80**, 4775 (1998).